Long-distance correlation-length effects and hydrodynamics of ^{4}He films in a Corbino geometry

Stephen R. D. Thomson,* Justin K. Perron,† and Francis M. Gasparini‡
Department of Physics, University at Buffalo, The State University of New York, Buffalo, New York 14260, USA
(Received 22 June 2016; revised manuscript received 9 August 2016; published 26 September 2016)

Previous measurements of the superfluid density ρ_s and specific heat for ^{4}He have identified effects that are manifest at distances much larger than the correlation length ξ_{3D} [Perron *et al.*, Nat. Phys. **6**, 499 (2010); Perron and Gasparini, Phys. Rev. Lett. **109**, 035302 (2012); Perron *et al.*, Phys. Rev. B **87**, 094507 (2013)]. We report here measurements of the superfluid density which are designed to explore this phenomenon further. We determine the superfluid fraction ρ_s/ρ from the resonance of 34-nm films of varying widths $4 \leqslant W \leqslant 100$ μm. The films are formed across a Corbino ring separating two chambers where a thicker 268-nm film is formed. This arrangement is realized using lithography and direct Si-wafer bonding. We identify two effects in the behavior of ρ_s/ρ: one is hydrodynamic, for which we present an analysis, and the other is a correlation-length effect which manifests as a shift in the transition temperature T_c relative to that of a uniform 34-nm film uninfluenced by proximity effects. We find that one can collapse both ρ_s/ρ and the quality factor of the resonance onto universal curves by shifting T_c as $\Delta T_c \sim W^{-\nu}$. This scaling is a surprising result on two counts: it involves a very large length scale W relative to the magnitude of ξ_{3D} and the dependence on W is not what is expected from correlation-length finite-size scaling which would predict $\Delta T_c \sim W^{-1/\nu}$.

DOI: 10.1103/PhysRevB.94.094520

I. INTRODUCTION

How do two coupled systems undergoing an ordering transition, which because of different constraints take place at different temperatures, affect each other? As reported by Perron *et al.* [1], the superfluid transition of an array of $(2\,\mu\text{m})^3$ boxes filled with ^{4}He and connected via a thin film show a remarkable action-at-a-distance coupling in the specific heat. This can be measured at a temperature corresponding to a distance of one hundred times the magnitude of the three-dimensional correlation length ξ_{3D}. Concomitant with this, the superfluid density ρ_s of the film connecting the boxes is influenced by the proximity to the boxes in two ways. Its superfluid transition is shifted closer to the bulk transition T_λ, and there is an overall enhancement of ρ_s above that of a uniform film of the same thickness [1–3]. It was conjectured by Perron and Gasparini [2] that such behavior might be generic to continuous phase transitions where fluctuations play an important role, and thus would not be limited to ^{4}He.

As remarked by Fisher [4], in the two-dimensional (2D) Ising system consisting of an array of strips with different coupling strengths there is also a two-peak structure in the specific heat, as is seen in the helium data [1], which is indicative of the role of the coupling strength between such strips. In more recent work [5,6] with 2D Ising strips of different spin coupling strengths and widths Au-Yang and Fisher found that there is an enhancement of the specific heat and of the overall critical temperature. In a calculation which more closely mimics the boxes-plus-film geometry, but still for 2D Ising, Abraham *et al.* [7] showed that there is a remarkable long-distance coupling between squares of spins connected through extraordinarily long linear links. This, they point out, is not a correlation-length effect but is associated with the emergence of a new length scale which diverges exponentially. Also, in experiments with junctions between two high-T_c superconductors through a link which is normal because of doping, tunneling is seen over distances much larger than the correlation length [8]. It seems that this, sometimes referred to as the giant proximity effect, is a manifestation of similar physics. There are no analogous calculations, as for the Ising system, for a 3D XY system as appropriate to ^{4}He. However, recent work has been reported by Del Maestro [9]. Mean-field calculations do not describe the effects seen [10].

In the case of low-temperature superconductors there have also been experiments which have shown long-range effects associated with the influence of one superconductor on another. Kwong *et al.* [11] have reported studies of the superconducting transition in aluminum films arrays in which the critical temperature in different regions is slightly different due to different chemical treatment. They find that the superconducting transition of the array shifts between the two temperature limits defined by the uniform films. However, when comparing this with expected theoretical predictions they find that they do not describe their data. The data indicate that a long-range coupling exists on a scale much larger than the correlation length, $\xi = 1$ μm for aluminum. They tentatively suggest that phase fluctuations due to the small $\sim$0.02 K difference in the transition temperature of the two regions might be responsible for this. In another series of measurements by Liu *et al.* [12], it was found that a single crystal of superconducting nanowires of length between 6 and 60 μm superconductivity was induced on the wires when in contact with superconducting electrodes of higher critical temperature. These authors also conclude that the observed long-range proximity effect cannot be understood by existing theories.

We report in this paper measurements of the superfluid fraction of ^{4}He confined as coupled films. The experiments have been designed to determine proximity effects on a thin film due to two adjoining superfluid regions which behave more

*st75@buffalo.edu
†Present address: California State University, San Marcos; jperron@csusm.edu
‡fmg@buffalo.edu

bulklike in the region where the thin film has its transition. The experimental arrangement consists of two regions where the ^{4}He is formed as a 268 ± 2-nm film. These regions are separated by, and linked through, a ring of controlled width where ^{4}He is formed as a 34.5 ± 0.5-nm film. This geometry is simpler than the arrangement of boxes-plus-film of the Perron *et al.* [1] experiments and is amenable to a more detailed analysis for the superfluid fraction. It also tests coupling in a different way: one two-dimensional film in proximity to another of different thickness.

This paper is organized as follows: we first describe the experimental arrangement; then we present a theory for the superfluid fraction for the geometry of the cells. This yields equations which do not include correlation-length effects but can be tested against the data, especially for the widest ring with $W = 100$ μm. This can be done without any adjustable parameters except for an overall magnitude normalization. More importantly, this theory also allows us to separate effects in ρ_s/ρ which are hydrodynamic in nature from effects of coupling which are correlation-length driven. We then present all of our data and further analysis. This is followed by conclusions.

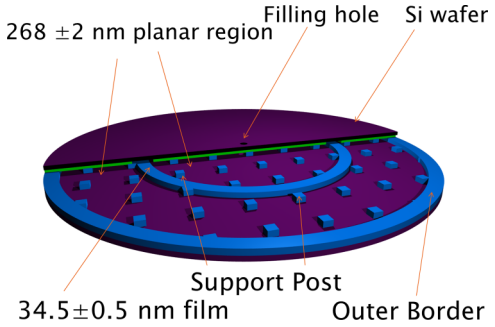

FIG. 1. A schematic rendering, not to scale, of the Corbino confinement. The cell is formed with two 50-mm-diameter silicon wafers. The support posts and outer border maintain wafer separation of 268 nm except over the Corbino ring of width W which has a 34-nm film above it. The 268-nm dimension was chosen since it is large enough so that in the region where the 34-nm film has its transition the 268-nm film has a superfluid fraction which is within 10% of the bulk value. The square posts $(100\,\mu\text{m})^2$ are at 200-μm separation and define the 268-nm separation of the two wafers inside and outside the Corbino ring. The 34-nm height is defined by the oxide pattern in the upper wafer.

II. EXPERIMENTAL DETAILS

The Corbino geometry [13] of our cells is depicted in Fig. 1 in a cutaway view. It consists of two silicon wafers 5 cm in diameter which have patterned oxide growths and are directly bonded [14,15]. The SiO_2 patterns in this cell consist of an outermost ring, which seals the cell, and an inner ring of 2.4 cm diameter which defines an opening of height $h = 34$ nm and width W. Not visible on this rendering is a series of oxide regions on the top wafer. These are bonded on the ring so that there are actually 250 openings across the ring each of 200 μm lateral width. This lateral dimension, as well as the height h are kept constant while W is varied for different cells. This design, with 1/3 of the ring area being bonded, ensures uniformity for the opening of small height h. The magnitude of h is chosen to match as closely as possible the film thickness used in the measurements with $(2\,\mu\text{m})^3$ boxes of helium, and in a separate experiment where the full cell consisted of a 33.6 ± 0.9-nm planar film [3,10]. These data will form a basis for comparison with the present results. The two regions surrounding the ring consist of a film which is $H = 268 \pm 2$ nm thick. See Table I for the actual dimensions h, H of each individual cell. This table also has the dimensions for other cells which are relevant for the present work. The height H is defined by bonding the wafers with a series of oxide posts which are $(100\mu\text{m})^2$ in cross section and at 200-μm separation. These posts take up 11% of the volume in these regions. The helium in the cell communicates with a filling line via a center hole. The staging of such a cell on a cryostat has been described previously [16]. Basically, it is an arrangement whereby excellent long-term temperature stability can be achieved by the use of a low-temperature valve to seal the filling line, and the use of three stages of temperature regulation. The cell is enclosed by two light shields, one anchored at a ^{4}He evaporator running at about 1.4 K, and another at a temperature a few mK above the temperature of the cell. A separate thermal link allows the cell to be regulated below the temperature of its light shield. More details can be found in [16]. The cell has a CuNi resistive film heater deposited in a spiral pattern on the outer surface of the bottom wafer. Two doped single-crystal Ge chips are

TABLE I. The oxide thicknesses for each Corbino cell and three other cells.

	Corbino cells	
W (μm)	Small oxide thickness (nm)	Large oxide thickness (nm)
4	34.1 ± 0.5	264.6 ± 1.0
8	34.4 ± 0.5	271.1 ± 1.3
18	34.6 ± 0.5	268.0 ± 1.1
18	34.8 ± 0.5	270.9 ± 1.1
40	34.6 ± 0.5	267.7 ± 0.8
100	34.4 ± 0.5	265.7 ± 0.9
Average	34.5 ± 0.5	268 ± 2
	Other cells [3]	
Uniform film thickness (nm)	33.6 ± 0.9	
Film with boxes (nm)	31.7 ± 0.1	(boxes at 4-μm separation)
Film with boxes (nm)	32.5 ± 1.2	(boxes at 2-μm separation)

epoxied to the top wafer. One is used to regulate the average temperature of the cell and the other to detect the temperature oscillations in response to an ac heating.

To obtain the superfluid fraction for the helium confined in this cell, or similar cells with different oxide patterns, one can apply a uniform ac heating and vary the frequency to search for resonant flow. The cells are a superleak sealed at one end. A resonance consists of superflow between the cell and the filling line. Because of the experimental arrangement this movement of the superfluid is adiabatic with very little heat flow between the cell and the filling line during the cycle of oscillation. This motion of the superfluid is accompanied with temperature and pressure excursions in the cell. We measure the temperature response. This technique has been described [17,18]. Our thermometry with a doped Ge chip enables us to resolve temperature oscillations within ∼50 nK. This is achieved by averaging the temperature oscillations over several minutes at fixed frequency. The range of resonant frequencies is typically between about 50 and 1000 Hz. The cell is held at a fixed average temperature for each resonance sweep. The normal fluid is viscously immobile. For a cell without the Corbino ring, there is a single Helmholtz resonance which has been called adiabatic fountain resonance (AFR) [17,18]. The analysis yields equations for the temperature oscillations and the phase shift of these oscillations relative to the ac excitation at the heater. In practice any superleak staged as the silicon cells will support an AFR resonance from which a value of the superfluid fraction can be obtained. However, the meaning of this superfluid fraction depends on the details of how the helium is confined. In the case of uniform films of thickness H the meaning is unambiguous: it is that of a film undergoing crossover from three dimensions to two dimensions as the superfluid transition is approached. In the case of the Corbino cells the meaning of the measured ρ_s requires some additional analysis.

There are no significant temperature gradients across the cell that can be determined experimentally. A calculation of the temperature distribution in the cell including details of the heater and thermal links shows that possible gradients are much less than one μK [19]. However, see below for an exception to this under a particular resonance condition.

In Figs. 2 and 3 we show two examples of resonances at two different temperatures. The data for the amplitude of the temperature oscillations are shown as the product of frequency times amplitude. This removes a dominant ω^{-1} dependence. The phase shift is that of the detected signal relative to the ac drive frequency. The lines through the data are a fit to the line shapes derived in [18]. We see in Fig. 2 that for $t \equiv (1 - T/T_\lambda) = 0.06$ both the phase and amplitude signals are fit well. They yield a consistent resonant frequency which is indicated by the vertical dashed line. In Fig. 3 are data for $t = 0.004$, much closer to the film's superfluid transition of $t_c \cong 0.003$; the fit to the phase is still good but the fit to the amplitude shows some systematic deviations. We believe that in this case the amplitude signal is distorted because of finite velocity effects. The maximum velocity for these particular data is 1 cm/s at the exit of the cell. In cases such as for Fig. 3 we rely only on the phase signal to determine the resonance. The increase of dissipation near the transition, above some noncritical background, is related to the process of vortex

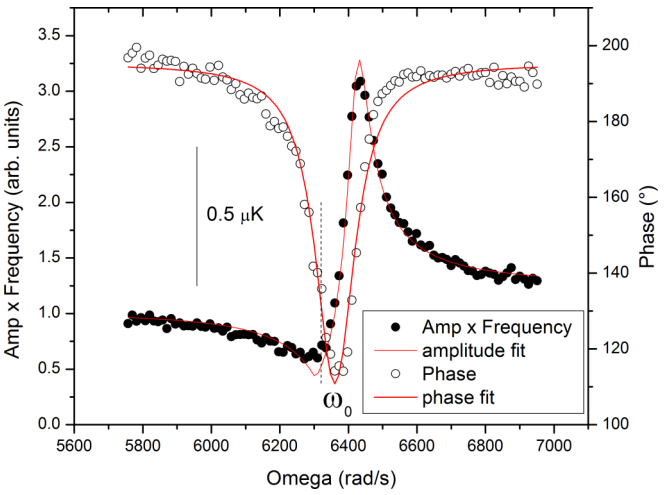

FIG. 2. A sample resonance signal for the amplitude and phase at $t = 0.06$ The data fit (solid lines) according to the adiabatic fountain resonance equations derived in [18]. The resonant frequency ω_0 is indicated by the dashed vertical line. The solid vertical line indicates the magnitude of the temperature oscillation.

pairs unbinding [20]. This affects the quality factor of the resonance and limits how close to the transition one can make a meaningful measurement. We note in these plots with a vertical line the magnitude of the temperature excursion for the amplitude signals. This depends on the frequency so it applies strictly to the region of the resonance. These temperature oscillations, as mentioned before, are not large, $\sim\pm 0.5$ μK. The temperature resolution of these oscillations can be inferred from the scatter of the amplitude data; it is better than 50 nK.

We present next a theory for the interpretation of the superfluid fraction which is determined from resonances with the Corbino cells.

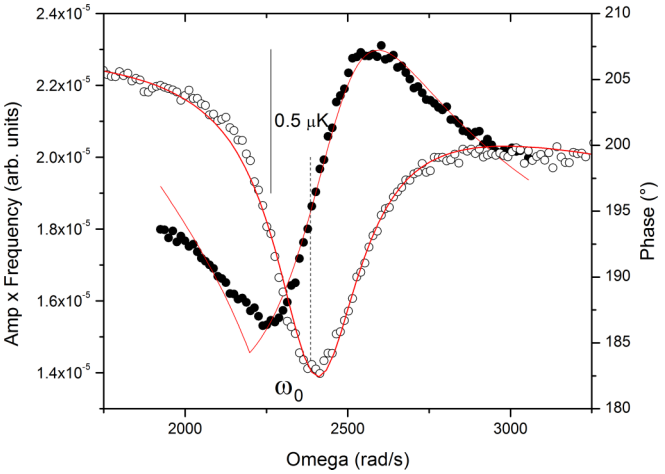

FIG. 3. A sample resonance signal for the amplitude and phase at $t = 0.004$. The data fit according to the adiabatic fountain resonance equations derived in [18]. Again, the resonant frequency is indicated by the dashed vertical line. The amplitude signal is somewhat distorted because of finite velocity effects, however the fit of the phase still yields the resonant frequency.

III. HELMHOLTZ RESONANCES FOR A THREE-CHAMBER OSCILLATOR

The superfluid fraction determined from a resonance with the Corbino cell with the widest ring $W = 100$ μm is shown in Fig. 4 on a log-log plot. Also shown in this figure are data for a cell with a uniform 33.6-nm film [3,10]. The solid line is the dependence of the superfluid fraction for bulk, unconfined helium [21]. Both sets of film data have the same critical temperature $t_c \cong 0.003$. The horizontal line is the magnitude for the expected Kosterlitz-Thouless jump [22] at t_c for a planar film of 33.6 nm. This can be written as

$$\Delta\rho_s = \frac{4m}{h\lambda_T^2}, \tag{1}$$

where $\lambda_T = 2\pi\hbar^2/mk_BT$ is the thermal wavelength, m is the mass of a ^{4}He atom, and h is the film thickness. One can see that the data for the 33.6-nm film comes close to this value; dissipation prevents following this closer than the last point. The data for a 34-nm film across a Corbino ring 100 μm wide and in equilibrium with a 268-nm film have a larger superfluid fraction but vanish effectively at the same temperature. The temperature dependence for the Corbino data is quite different from that of a planar film. This is brought out more clearly in Fig. 5 where the ratio of $\rho_s/\rho_{s,\mathrm{bulk}}$ is plotted. Both of these data are normalized to the bulk value near $t = 0.1$. The decrease from this value as one moves closer to the transition is quite different for these two cases. The Corbino data fall quite abruptly at the critical temperature near $t_c \cong 0.003$, while the uniform film has a more gentle decrease toward t_c. To understand this behavior we examine now in more detail the resonances allowed for the Corbino cells and hence an interpretation of the behavior shown in Fig. 5.

Rayleigh considered Helmholtz resonances in a two-chamber gas oscillator with open ends [23]. The approach is to construct a Lagrangian involving the kinetic energy of the gas and the potential energy associated with the compressibility. In the same spirit one can view the Corbino cells as a three-chamber radial oscillator which is however closed on one end and open at the center. The three chambers consist of the two chambers where the helium film is at a thickness $H = 268$ nm; we will refer to these as regions 1 and 3, with chamber 1 open to the filling line. Chamber 2 is the region across the ring where the film is at $h = 34$ nm. To just focus on the possible resonances, one can ignore dissipation in the movement of the superfluid and construct a Lagrangian from which the equations of motion follow. Given the confinement dimensions and the frequencies in the experiment (the viscous penetration depth is of the order of 25 times the largest separation of the silicon surfaces) only the superfluid component will flow. The kinetic energy can then be written as

$$\mathrm{KE} = \tfrac{1}{2}g_0\rho_{sb}\dot{r}_1^2 + \tfrac{1}{2}g_1'\rho_{s1}\dot{r}_1^2 + \tfrac{1}{2}g_2\rho_{s2}\dot{r}_2^2 + \tfrac{1}{2}g_3\rho_{s1}\dot{r}_3^2, \tag{2}$$

where $\dot{r}_i$ is the velocity of the superfluid at the entrance of each chamber and g_i is a geometric factor with units of volume reflecting the radial flow in the cell. The first term is introduced as an end correction to include the fact that the superfluid flows out of the cell (and into a fourth chamber, the filling line which is at saturated vapor pressure) with a velocity $\dot{r}_1$ and at the bulk superfluid density ρ_{sb}. The superfluid densities in chambers 1 and 3 are the same ρ_{s1}, characteristic of the 268-nm confinement plus any influence from ρ_{s2} in the ring. The end-effect volume g_0 can be determined from hydrodynamics. It has been shown that for flow out of a channel through a flanged orifice the effective length of the channel is increased by an amount given by $\delta\ell = 0.48\sqrt{A}$, where A is the cross-sectional area of flow [24,25]. This length turns out to be small relative to the overall linear dimension of the cell: with $R = 2$ cm one finds $\delta\ell/R = 0.7 \times 10^{-3}$. However, at the exit of the cell the superfluid velocity is largest, and it is more realistic to include this end effect as an additional kinetic energy. One has $g_0 = 2\pi r_0 H\delta\ell = 1.20 \times 10^{-8}$ cm^3 where $r_0 = 0.0508$ cm is the radius of the opening into the silicon cell, and from the above $\delta\ell = 1.4 \times 10^{-3}$ cm. Note that this end correction is much smaller than the one considered by Brooks *et al.* [26] for a Helmholtz resonator

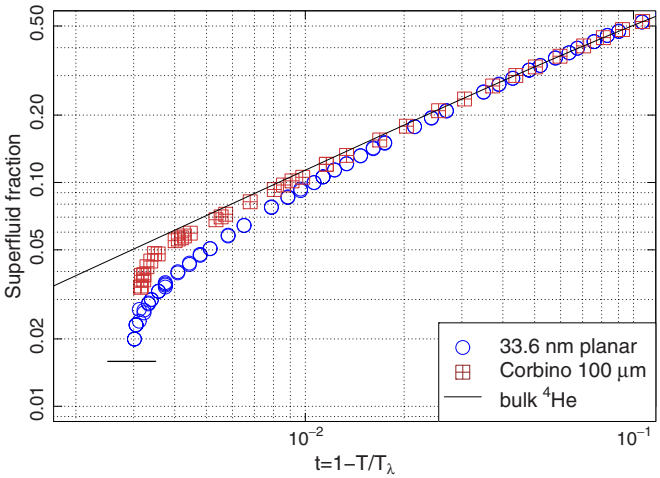

FIG. 4. The superfluid fraction of the Corbino cell with $W = 100$ μm is shown with the 33.6-nm planar data. A hydrodynamic effect causes the Corbino data to behave like a 268-nm film until near t_c where there is a rapid decrease in the superfluid fraction.

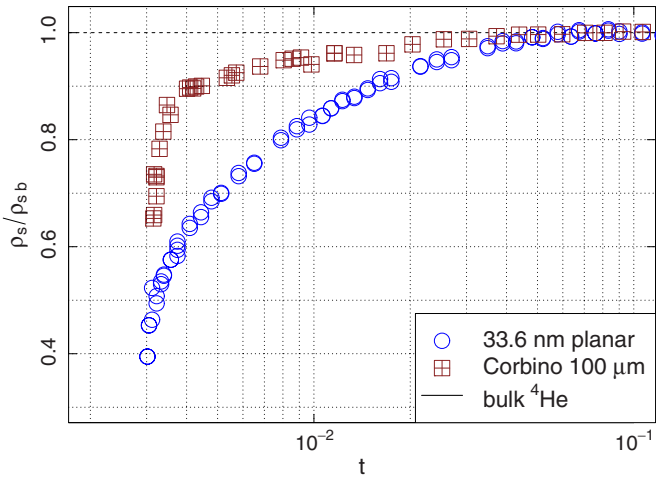

FIG. 5. The ratio ρ_s/ρ_{sb} vs t for the Corbino cell with $w = 100$ μm, and the 33.6-nm planar data. The difference in the behavior of these data can be understood via the hydrodynamics discussed below.

involving an array of channels in Nuclepore filters [27–29] separating two chambers of bulk helium. The other geometric factors can be obtained by assuming a $1/r$ velocity field inside the cell. In chamber 1 this extends from r_0 to the Corbino ring $R_c = 1.2$ cm, $\dot{r}(r) = \dot{r}_1 \times (\frac{r_0}{R-r_0})(\frac{R}{r} - 1)$. With this dependence of the velocity on the radial distance, the total kinetic energy in this chamber is given by

$$\mathrm{KE}_1 = \frac{1}{2}\rho_{s1}\dot{r}_1^2\left\{2\pi f_1 H\left(\frac{r_0}{R-r_0}\right)^2 \times\left[R^2 \ln\frac{R_c}{r_0} - 2R(R_c - r_0) + \frac{1}{2}\left(R_c^2 - r_0^2\right)\right]\right\}, \quad (3)$$

where $f_1 = 0.89$ is the open fraction of this chamber not taken up by the supporting oxide posts. One finds $g_1' = 8.8 \times 10^{-7}$ cm^3. Similarly, for region 3 extending from R_c to $R = 2.0$ cm, one can take the velocity field as $\dot{r}(r) = \dot{r}_3 \times (\frac{R_c}{R-R_c})(\frac{R}{r} - 1)$. Upon integration from R_c to R one finds $g_3 = 4.11 \times 10^{-5}$ cm^3. For the chamber defined by the relatively narrow width and height of the Corbino ring, one can take the velocity field as constant. One has $g_2 = V_2 = f_2 2\pi R_c H W$ where $f_2 = 2/3$ is the fraction of the volume which is not taken up by the oxide supports in this region, and W is the width which we will take for the present numerical calculation as the largest we have used in our cells: 100 μm. One finds $g_2 = 1.73 \times 10^{-7}$ cm^3.

One can now incorporate the end correction into a single term so that KE_1 is given by

$$\mathrm{KE}_1 = \frac{1}{2}g_0\rho_{sb}\dot{r}_1^2 + \frac{1}{2}g_1'\rho_{s1}\dot{r}_1^2 = \frac{1}{2}\rho_{s1}g_1'\left(1 + \frac{g_0}{g_1'}\frac{\rho_{sb}}{\rho_{s1}}\right)\dot{r}_1^2 = \frac{1}{2}g_1'\left(1 + 1.36 \times 10^{-2}\frac{\rho_{sb}}{\rho_{s1}}\right)\rho_{s1}\dot{r}_1^2 \equiv \frac{1}{2}g_1\rho_{s1}\dot{r}_1^2. \quad (4)$$

The potential energy U is due to the compression and rarefaction of the confined helium and the flexing of the 375-μm-thick Si wafers as the superfluid moves between chambers. It is given by

$$U = \frac{1}{2K_1V_1}(v_1 - v_2)^2 + \frac{1}{2K_2V_2}(v_2 - v_3)^2 + \frac{1}{2K_3V_3}v_3^2 \quad (5)$$

where v_i represents the volume entering each chamber, and K_i, V_i are the compressibility and volume of each chamber. The volumes entering the chambers can be written as $v_1 = \Delta r_1\sigma_1\frac{\rho_{s1}}{\rho}$; $v_2 = \Delta r_2\sigma_2\frac{\rho_{s2}}{\rho}$; $v_3 = \Delta r_3\sigma_3\frac{\rho_{s1}}{\rho}$. The variables $\Delta r_i = r - r_i$ are the displacement of the superfluid measured from the entrance of each chamber. The cross-sectional areas of flow σ_i and the volumes of each chamber v_i are given in Table II. The equations of motion now follow from the Lagrangian $\mathrm{KE} - U$,

$$\ddot{r}_1 + \alpha\rho_{s1}\Delta r_1 - \alpha_{12}\rho_{s2}\Delta r_2 = 0, \quad (6)$$

$$\ddot{r}_2 - \alpha_{122}\rho_{s1}\Delta r_1 + \beta\rho_{s2}\Delta r_2 - \alpha_{232}\rho_{s1}\Delta r_3 = 0, \quad (7)$$

$$\ddot{r}_3 - \alpha_{233}\rho_{s2}\Delta r_2 + \gamma\rho_{s1}\Delta r_3 = 0, \quad (8)$$

where the coefficients of Δr_i involve various geometric factors and the compressibilities. These factors are listed in Table III. Assuming an oscillatory solution $\Delta r_i = \Delta r_{io}e^{i\omega t}$ yields the following secular equation for the angular frequency:

$$\omega^6 - [\beta\rho_{s2} + (\alpha + \gamma)\rho_{s1}]\omega^4 + \left[(\gamma\beta + \alpha\beta - \alpha_{232}\alpha_{233} - \alpha_{12}\alpha_{122})\rho_{s1}\rho_{s2} + \alpha\gamma\rho_{s1}^2\right]\omega^2 - (\alpha\beta\gamma - \alpha\alpha_{232}\alpha_{233} - \alpha_{12}\alpha_{122}\gamma)\rho_{s1}^2\rho_{s2} = 0. \quad (9)$$

This equation allows for three solutions in ω^2. The simplest is when $\rho_{s2} = 0$ across the Corbino ring, in which case there is no flow from the outer volume and the term γ must also be set to zero. This leaves only a resonance associated with V_1 and is given by

$$\omega_0^2 = \alpha\rho_{s1} = \frac{\sigma_1^2}{g_1K_1V_1\rho}\frac{\rho_{s1}}{\rho}. \quad (10)$$

This can be compared with the expression obtained from the AFR analysis [18],

$$\omega_{\mathrm{AFR}}^2 = \frac{\sigma_1}{lK_1V_1\rho}\frac{\rho_{s1}}{\rho}. \quad (11)$$

In the AFR derivation a more realistic length l is introduced to take into account the length over which the temperature T and pressure P vary from their oscillating values in the cell to the constant values in the filling line. The filling line contains about one mm^3 of bulk helium. In practice l can be obtained from the measurements only if $K_1 = K_{\mathrm{He}} + K_{\mathrm{Si}}$ is known. It

TABLE II. Geometric terms for $W = 100$ μm Corbino cell.

Radius of filling hole	$r_1 = 0.0508$ cm
Radius of Corbino ring	$R_c = 1.20$ cm
Volume of chamber 1	$V_1 = 1.07 \times 10^{-4}$ cm^3
Volume of Corbino ring	$V_2 = 1.73 \times 10^{-7}$ cm^3
Volume of chamber 3	$V_3 = 1.90 \times 10^{-4}$ cm^3
Cross section into chamber 1	$\sigma_1 = 8.5 \times 10^{-6}$ cm^2
Cross section into chamber 2	$\sigma_2 = 1.73 \times 10^{-5}$ cm^2
Cross section into chamber 3	$\sigma_3 = 2.00 \times 10^{-4}$ cm^2
KE factor for end correction	$g_0 = 1.20 \times 10^{-8}$ cm^3
KE factor for chamber 1	$g_1 = 8.8 \times 10^{-7} \times \delta$ cm^3
KE factor for chamber 2	$g_2 = 1.73 \times 10^{-7}$ cm^3
KE factor for chamber 3	$g_3 = 4.11 \times 10^{-5}$ cm^3

TABLE III. Terms in the secular equation with $W = 100$ μm. Units are in cm^{-2} except as noted; δ is dimensionless.

$\alpha = \sigma_1^2/(K_1\rho^2 g_1 V_1) = 0.77/K_1\rho^2\delta$
$\beta = \sigma_2^2/(K_2\rho^2 g_2 V_2) + \sigma_2^2/(K_1\rho^2 g_2 V_1) \cong 0.99 \times 10^4/K_2\rho^2$
$\gamma = \sigma_3^2/(K_2\rho^2 g_3 V_2) + \sigma_3^2/(K_3\rho^2 g_3 V_3) \cong 5.6 \times 10^3/K_2\rho^2$
$\alpha_{12} = \sigma_1\sigma_2/(K_1\rho^2 g_1 V_1) = 1.55/K_1\rho^2\delta$
$\alpha_{122} = \sigma_1\sigma_2/(K_1\rho^2 g_2 V_1) = 7.9/K_1\rho^2$
$\alpha_{233} = \sigma_2\sigma_3/(K_2\rho^2 g_3 V_2) = 4.8 \times 10^2/K_2\rho^2$
$\alpha_{232} = \sigma_2\sigma_3/(K_2\rho^2 g_2 V_2) = 1.15 \times 10^5/K_2\rho^2$
$\alpha(\beta\gamma - \alpha_{232}\alpha_{233}) - \alpha_{12}\alpha_{122}\gamma$
$= (\sigma_1\sigma_2\sigma_3)^2/(K_1K_2K_3\rho^6 g_1 g_2 g_3 V_1 V_2 V_3)$
$= 3.9 \times 10^4 \mathrm{cm}^{-6}/K_1K_2K_3\rho^6\delta$
$\delta = 1 + 0.0136\rho_{sb}/\rho_{s1}$

is found from many cells for which this resonance has been studied and from the magnitude of the resonant frequencies of these cells, that $K_1 \gtrsim K_{\rm He}$. $K_{\rm Si}$ depends on the oxide pattern, the uniformity of the bonding and the thickness of the wafers, 375 μm in our case. Thus, to take care of the unknown values of K_1 and l the superfluid fraction obtained from the measured resonance is normalized in a region of temperature where confinement effects are negligible, i.e., where the ratio of the data to the corresponding bulk superfluid fraction is 1. In this way only the combination of factors σ_1/lK_1 is determined. The AFR derivation also has the advantage that dissipation is included and expressions for the resonant line shapes can be obtained [18]. However, the existence of an AFR resonance simply indicates that there is adiabatic superflow in a superleak which is accompanied by temperature oscillations of the enclosure. It says nothing about the possible structure within that superleak or the meaning of the observed superfluid fraction relative to this internal structure. The Lagrangian derivation supplements the AFR by determining the meaning of the measured ρ_s in terms of the detailed structure of the superleak. Another aspect of the Lagrangian approach is the ability to introduce an end correction in a meaningful way.

It is interesting to use this end correction to gauge the effect on a cell which is fully a 34-nm film. One finds that the correction is small and given by $\delta = (1 + 4.2 \times 10^{-3}\rho_{sb}/\rho_{s,\rm film})$. This would imply a maximal correction of less than two percent from the value $\rho_{s,\rm film}/\rho_{s,b} \cong 1$ well below the transition, to the point closest to the transition temperature where the lowest value measured is $\rho_{s,\rm film}/\rho_{s,b} \cong 0.3$.

For the region where both superfluid fractions are nonzero, evaluation of the various terms in the secular equation shows that for typical experimental frequencies the ω^6 term is smaller than the other terms in the equation by six to eight orders of magnitude. The ω^6 term would become important at frequencies above 10^4 Hz which are not realized experimentally. Thus, the ω^6 term can be dropped and the equation becomes a quadratic in ω^2 with solutions given by

$$\omega_\pm^2 = -\frac{b}{2a} \pm \frac{b}{2a}\sqrt{1 - \frac{4ac}{b^2}}, \tag{12}$$

$$a = \beta\rho_{s2} + (\alpha + \gamma)\rho_{s1}, \tag{13}$$

$$b = (-\gamma\beta - \alpha\beta + \alpha_{232}\alpha_{233} + \alpha_{12}\alpha_{122})\rho_{s1}\rho_{s2} - \alpha\gamma\rho_{s1}^2, \tag{14}$$

$$c = (\alpha\beta\gamma - \alpha\alpha_{232}\alpha_{233} - \alpha_{12}\alpha_{122}\gamma)\rho_{s1}^2\rho_{s2}. \tag{15}$$

From the above one can see that in the limit that the superfluid density in the ring becomes small one can expand the square root to obtain

$$\omega_-^2 = -\frac{c}{b} = \frac{(\alpha\beta\gamma - \alpha\alpha_{232}\alpha_{233} - \alpha_{12}\alpha_{122}\gamma)\rho_{s1}\rho_{s2}}{[(\gamma\beta + \alpha\beta - \alpha_{232}\alpha_{233} - \alpha_{12}\alpha_{122})\rho_{s2} + \alpha\gamma\rho_{s1}]}. \tag{16}$$

Thus ω_- will vanish as ρ_{s2} vanishes. One can now identify this resonance, which vanishes at $t_c = 0.003$, as characteristic of the 34-nm film. This resonance will track the vanishing of ρ_{s2}, but obviously will have contributions from ρ_{s1} as given by this equation as one moves to lower temperatures. The other solution ω_+^2 does not vanish when ρ_{s2} vanishes but has a strong dip as ρ_{s2} goes to zero. This is the resonance dominated by the two 268-nm chambers which eventually must cross over to a single chamber resonance as ρ_{s2} vanishes. We were able to excite this second resonance only for the Corbino ring with $W = 40$ μm. See below.

One can replace the various terms in the secular equation with their numerical values. These are known for the patterned cells to within a few percent. The largest uncertainty is for the filling hole in the center of the cell which is made with a 0.040-in. diameter diamond drill. The effective hole size is probably known within 10% . With numerical values, and for the case of the $W = 100$-μm-wide ring, the expression for the resonance ω_- across the ring is given by

$$\frac{\omega_-^2}{\frac{4.5\rm cm^{-2}\rho_{sb}}{K_1\rho^2}} = \left[\frac{\left(1 + 0.56\frac{K_1}{K_3} + \frac{0.084}{\delta}\right)\rho'_{s1}\rho'_{s2} + \frac{0.048}{\delta}\rho'^2_{s1}}{\rho'_{s2} + 0.57\rho'_{s1}}\right]\left[1 - \sqrt{1 - 0.19\frac{\left(\rho'_{s2} + 0.56\rho'_{s1}\right)\rho'_{s2}\frac{1}{\delta}\frac{K_1}{K_3}}{\left[\left(1 + 0.56\frac{K_1}{K_3} + \frac{0.084}{\delta}\right)\rho'_{s2} + \frac{0.048}{\delta}\rho'_{s1}\right]^2}}\right], \tag{17}$$

where $\delta = (1 + 1.36 \times 10^{-2}\frac{\rho_{sb}}{\rho_{s1}})$ is the end correction. The compressibilities for regions 1 and 3 are retained in this expression. One expects that $K_1/K_3 \cong 1$ given that both regions have the same 11% of oxide bonding. The ring region with 33% bonding is expected to have a much smaller compressibility with $K_2 \cong K_{\rm He}$. This cancels out in the above. Finally, we note that because we analyze the data as the ratio of the measured superfluid fraction normalized by the bulk value, we have done so in the above expression with the notation $\rho'_{si} \equiv \rho_{si}/\rho_{s,\rm bulk}$.

The left hand side of the above is the quantity $\rho_{s,\rm measured}/\rho_{s,\rm bulk}$. We can see that it is a function of both the superfluid fraction on the two sides of the ring ρ_{s1}, and the superfluid fraction across the ring ρ_{s2}. To test this equation against the measured value one needs ρ_{s1} and ρ_{s2}. One can assume that with $W = 100$ μm ρ_{s2} will be well represented by that of a uniform film. One has available data from an independent experiment where the full volume of the cell was at 33.6 nm. This can be used with no adjustments. The small difference in h of about 1 nm between these data and the present data is not important. It would cause, for instance, a difference in the value of t_c of 0.000 02, about two orders of magnitude smaller than t_c itself. The difference in h is also within the uncertainty of the determination of the oxide thickness.

For ρ_{s1} there are no available data. However, one can construct the behavior of ρ_{s1} from experimental measurements of a film of thickness $H = 0.2113$ μm [30]. Even though the data for the superfluid density do not scale with size as $tH^{1/\nu}$ over a wide range of H [31], one can still use this scaling for

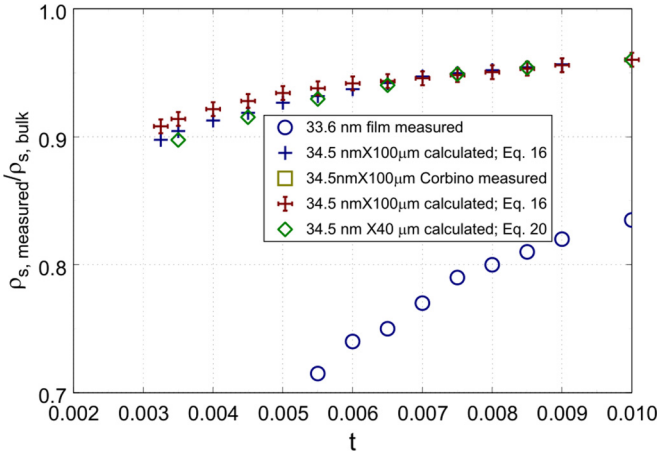

FIG. 6. The ratio ρ_s/ρ_{sb} vs t for the Corbino cell with $w = 100\ \mu$m and the 33.6-nm planar data are plotted with the calculated values for the Corbino cell. The calculated values for this quantity are the pluses using the data from ω_+ of the 40-μm ring, and the crosses using ρ_{s1}(268 nm) from the scaled value of ρ_{s1} (0.2113 μm). The diamonds are calculated using an internal cell resonance, Eq. (20). See text.

small variations in H; see for instance [32]. An alternative to this is to use the superfluid density we obtained from the second resonance ω_+ with a 40-μm ring. This follows ρ_{s1} (268 nm) but is affected by the behavior of ρ_{s2} near the transition in the region where ρ_{s2} vanishes. However, as we will see, with the 40-μm ring the transition is at slightly warmer temperature than for 100-μm ring. Thus using the results from ω_+ is not unreasonable. We show the results of this calculation of $\rho_{s,\mathrm{measured}}/\rho_{s,\mathrm{bulk}}$ via Eq. (17) in Fig. 6. The measured values of the superfluid fraction for the 100-μm ring obtained from ω_- are the open squares. The calculated values for this quantity are the pluses using the data from ω_+ of the 40-μm ring, and the crosses using ρ_{s1} (268 nm) from the scaled value of ρ_{s1}(0.2113 μm). The open circles are the data for the uniform 33.6-nm film. Both the calculated values and the measured data go to zero at $t \cong 0.003$ as expected from Eq. (17). The two ways of calculating $\rho_{s,\mathrm{measured}}/\rho_{s,\mathrm{bulk}}$ agree quite well. Both reproduce the relatively shallow drop in $\rho_{s,\mathrm{measured}}/\rho_{s,\mathrm{bulk}}$ away from t_c, but miss in the region where $\rho_{s,\mathrm{measured}}/\rho_{s,\mathrm{bulk}}$ goes rapidly to zero, i.e., the calculated values have a much sharper, almost discontinuous, drop to zero than the data. This might have been expected. The data reflect the rapid onset of dissipation near the transition and display a relatively smooth but still sharp reduction of the superfluid fraction. The calculated superfluid density drops almost discontinuously to zero at $t_c \cong 0.003$. There is no dissipation in the Lagrangian model, so this difference is not surprising. The important result of this calculation is the fact that the model reproduces the large enhancement of $\rho_{s,\mathrm{measured}}/\rho_{s,\mathrm{bulk}}$, the difference between the open circles and the measured data, the open squares in the region just below the transition. Thus this feature is not due to correlation-length effects between the film across the ring and the films external to it, but rather is a hydrodynamic effect of this particular cell arrangement of superleaks. We will see that this feature will also be present with data for narrower rings. However, these will in addition show an enhancement in t_c which will be the indication of correlation-length effects between the films.

We note that the above results are independent of the end correction. This correction, which can be inferred from Eq. (17) by setting $\delta = 1$, has less than a 0.1% effect in the change of the superfluid fraction in the region $0.003 \leqslant t \leqslant 0.01$. Thus it is negligible. The dependence of the superfluid fraction on the ratio of the compressibilities K_1/K_3 can also be tested. Varying this ratio in the range 10–0.1 changes the results by $\pm 1\%$ of the drop in the superfluid fraction in the region $0.003 \leqslant t \leqslant 0.01$. Smaller values of this ratio have a negligible effect. It is very likely, as pointed out above, that, given the construction of the cell with the same oxide bonding in regions 1 and 3, one will have $K_1/K_3 \cong 1$. This is the value used for the calculations shown in Fig. 6.

In summary, the model for the interpretation of the measured superfluid fraction in these cells obtained from the resonance ω_- shows that the region below the transition temperature of the 0.034-μm film across the Corbino ring is dominated by the behavior of the 0.27-μm regions on either side of the ring. For the ring of 100 μm there are no discernible correlation-length effects associated with critical coupling between these two regions as would be evidenced by a shift in the critical temperature relative to that of a uniform film.

It is interesting to consider the above results for confinements which are much more complicated than the Corbino geometry considered above, say a cell with a distribution of sizes such as would be realized with packed powders superleaks or with porous glasses. It seems clear that the interpretation of such data from a resonance measurement would not be straightforward. It would reflect the confinement in a unique way which could not be generalized from sample to sample or be indicative of a type of universal behavior.

IV. DATA WITH NARROWER CORBINO RINGS

We have obtained data for six different experimental cells each with the same 34.5 ± 0.5-nm thickness film across the ring and with width $W = 4, 8, 18, 40$, and 100 μm. In the case of the 18-μm ring we constructed and measured two separate cells to verify the reproducibility of the cell construction and the subsequent measurements.

Among all of these cells the one with a 40-μm ring behaved differently. This was the only cell for which we were able to excite the resonance ω_+. This is given by Eq. (17) only with the plus sign in front of the square root. Of course there are slightly different constants reflecting the ring being 40 μm wide as opposed to 100 μm wide. These data are shown in Fig. 7 as crosses. Also shown on this plot are data of ρ_s for a uniform 268-nm film obtained by scaling the data from the measured ρ_s of a 211-nm film. One can see that the measured value of ρ_s obtained from ω_+ agrees with the behavior of a 268-nm film except in the region where ρ_{s2} goes to zero near $t \cong 0.0035$. Here the measure ρ_s has a dip which is predicted by ω_+. In principle we should be able to calculate this behavior from ω_+. However, contrary to the 100-μm ring there is a shift in the critical temperature of the film in the ring. Thus it would not be correct to assume that ρ_{s2} within the ring could be represented by that of a uniform film. The motion of the helium

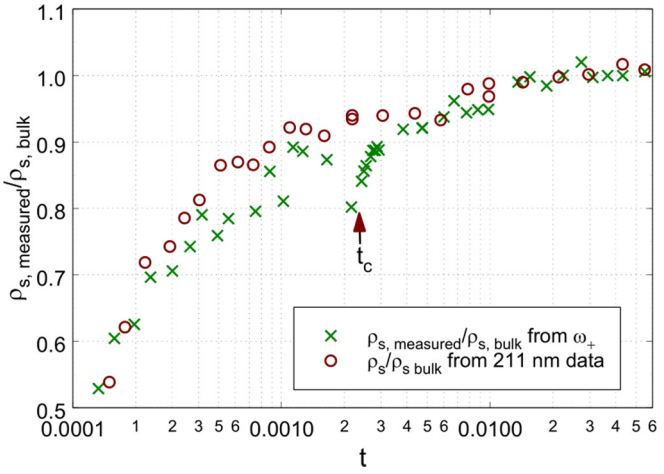

FIG. 7. The ratio ρ_s/ρ_{sb} vs t for the Corbino cell with $w = 40\ \mu$m obtained from ω_+, and the data for 211-nm planar film scaled to 268 nm.

for the ω_+ mode must be different from that of the ω_- mode. In the latter, helium moves in phase in all chambers, in and out of the cell. For ω_+, helium must still move out of the cell from chamber V_1 since, with typical excitation levels, we see a "normal" amplitude of temperature oscillations corresponding to a few μK. However, it is possible that in chamber V_3 the helium moves out of phase with respect to the motion in V_1. We have no way to establish this from the data.

There is another possibility for a resonance which would not involve helium leaving the cell. This would be an internal mode where the movement of the helium is out of phase in the two chambers with a velocity node at the filling line, the outer cell border, and in the middle of the ring. We have measured such a mode with the 40-μm cell. The characteristics of this internal mode are a much smaller temperature signal of ~200 nK, and a resonance at a higher frequency than given by Eq. (17). The difference is that this new motion conserves mass within the cell. Consequently, because of this constraint, one obtains a secular equation which is second order in ω^2. The solution for ω^2 which vanishes when ρ_{s2} vanishes is given by

$$\omega_H^2 \cong \frac{\sigma_3^2\rho_{sb}}{(g_1+g_3)K_1V_1\rho^2}\left(1+\frac{K_1V_1}{K_3V_3}\right)\frac{\rho'_{s1}\rho'_{s2}}{\rho'_{s2}+\frac{3g_2}{g_1+g_3}\frac{\sigma_3^2}{\sigma_2^2}\rho'_{s1}}. \tag{18}$$

This is obtained with the assumption that $K_2V_2 \ll K_1V_1, K_3V_3$. The symbols in the above have the same values as in the case of the derivation of Eq. (17), except for g_i which can only be determined if one knows the velocity dependencies within each chamber of the cell. One could also look at this resonance as a fourth sound mode [33]. However, this would not allow one to sort out the contributions of the measured superfluid density from the different regions of the cell. The structure of Eq. (18) is the same as Eq. (17). This can be seen by expanding the square root in Eq. (17) and retaining the symbols as Eq. (18). One obtains

$$\omega_-^2 \cong \frac{\sigma_1^2\rho_{sb}}{g_1K_1V_1\rho^2}\frac{\rho'_{s1}\rho'_{s2}}{\left[1+\frac{K_3V_3}{K_1V_1}\left(1+\frac{g_3\sigma_1^2}{g_1\sigma_3^2}\right)\right]\rho'_{s2}+\frac{K_3V_3}{K_1V_1}\frac{g_2\sigma_1^2}{g_1\sigma_2^2}\rho'_{s1}}, \tag{19}$$

where one has assumed $K_2V_2 \ll K_1V_1, K_3V_3$ and we have omitted the end correction. One can see that the dependence of these two frequencies ω_H, ω_- on ρ_{s1}, ρ_{s2} is the same, both vanishing when ρ_{s2} vanishes. One can go further by assuming that $K_1 = K_3$, and for Eq. (18) approximating the velocity field as decreasing linearly to zero within the ring and at the edges. This allows one to calculate the g factors. For Eq. (19) all the factors are the same as in Table II, except for g_2 which for 40 μm is 2.5 times smaller. One can now display Eq. (18) with numerical factors

$$\omega_H^2 \sim \frac{\rho'_{s1}\rho'_{s2}}{\rho'_{s2}+0.042\rho'_{s1}}. \tag{20}$$

This equation is plotted as the diamonds in Fig. 6 using as an approximation the values for ρ_{s1}, ρ_{s2} of planar films. This procedure is not strictly valid but is reasonable to see the behavior of the measured ρ_s as one approaches the transition. One can see that the behavior predicted by Eq. (20) and this different resonance mode is very similar to that predicted for ω_- by the full Eq. (17). Thus, we conclude that we can use these data from this internal mode at equal footing with all the other data which are obtained with the resonance ω_-.

We note that if we use Eq. (18) to compare the magnitude of the measured frequency one would require that $K_1 \cong 9 \times K_{\rm He}$ for the 40 μm cell. For the other cells, and the magnitude of ω_-, one finds that $K_1 \cong 1.26 \times K_{\rm He}$. This is consistent with the assumption that $K_1 > K_{\rm He}$ we have been making all along in describing these resonances.

For each cell the procedures followed after bonding, staging on the cryostat and data acquisition were the same. In particular, for each cell a separate temperature calibration of the Ge thermometers was done. This is required because the bare Ge chips do not maintain their calibration upon recycling. More importantly, since the relevant variable is $t \equiv (1 - T/T_\lambda)$, for each cell a determination of the bulk superfluid transition was done several times over the course of the measurements. To obtain T_λ one makes use of the maximum in the heat capacity associated with a small bulk sample which is condensed in the cell's filling line. This procedure is described in [16]. For each cell a series of resonances is obtained. These, as discussed, are proportional to $\sqrt{\rho_s/\rho}$ but need to be normalized to $\rho_{s,\rm bulk}$ far from the transition because of the uncertainty in the compressibility. The complete set of data is shown on the log-log plot in Fig. 8. The behavior of $\rho_{s,\rm bulk}/\rho$ is given by the solid line [21]. All of the data are for the same resonance ω_- (ω_H in the case of 40 μm), except for the ×'s which are for ω_+. The remarkable aspect of these data is that even with W as large as 40 μm one can see a measurable shift of the transition closer to T_λ due to the presence of the 268-nm film on either side of the ring. Since there are supports over the ring which separate the film into 200-μm-wide sections, one may look at the Corbino film as one consisting of 250 sections with dimensions $0.034 \times W \times 200\ \mu\text{m}^3$ with Dirichlet boundary conditions along the direction perpendicular to the flow at $L = 200\ \mu$m defined by the bonded SiO_2; and, order-parameter-matching conditions in the direction of flow W. With lateral dimensions of $W \times 200\ \mu\text{m}^2$ one might well consider this patch of film as having infinite lateral extent, at least based on the magnitude of $\xi_{3D}^- = \xi_0^- t^{-\nu} = 0.353 t^{-\nu}$ nm $\cong 17$ nm at $t = 0.003$. Thus,

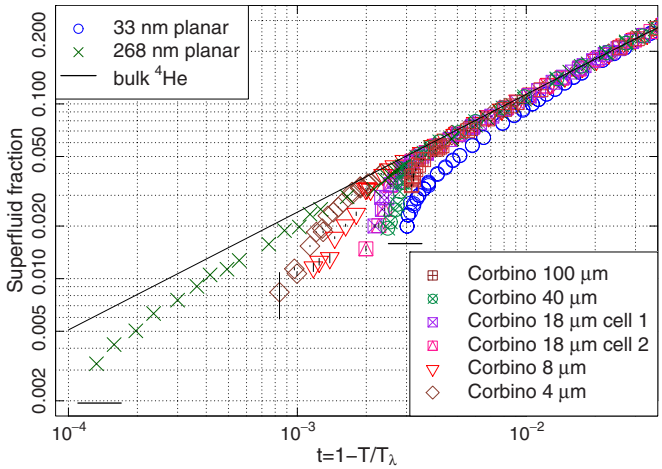

FIG. 8. The superfluid fraction ρ_s/ρ vs the reduced temperature t. The open circles are the 33-nm planar data to which the Corbino data are compared. The two horizontal lines are the expected Kosterlitz-Thouless jump for the 33.6- and 268-nm planar data.

one has $W/\xi_{3D}^{-} \cong 2400$ to 240 for the range of W's where a shift in t_c is measured. These are very large distances for correlation-length effects. The temperature dependence of these data in Fig. 8 does not appear at first to be much different from other data of confined helium. However, as we have seen from Figs. 4 and 5 for the case of $W = 100$ μm this can be deceptive on a log-log plot which does not have sufficient resolution. In Fig. 9 we show all of the data plotted as $\rho_s/\rho_{s,\mathrm{bulk}}$. This type of plot takes away what one might consider a background temperature dependence of the bulk superfluid density. The shift in the transition temperature is more obvious here as is the difference in the temperature dependence of the Corbino data relative to that of the planar 33.6-nm film, the open circles. All the Corbino data have the characteristic which we identified in Fig. 5 and via Eq. (17) as a hydrodynamic effect between the 34-nm film and the 268-nm film on either side of ring: below the transition, colder temperatures, the value of ρ_s follows more closely the behavior of the 268-nm film. Now,

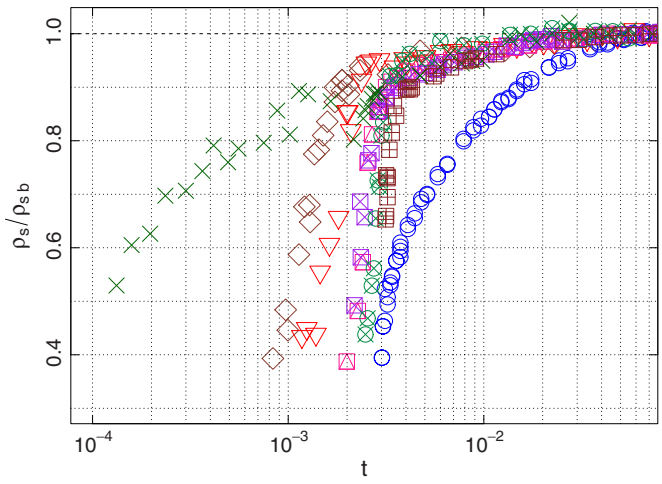

FIG. 9. The ratio ρ_s/ρ_{sb} vs t for all the Corbino cells and for the 33.6-nm planar data. The symbols are identified in Fig. 8.

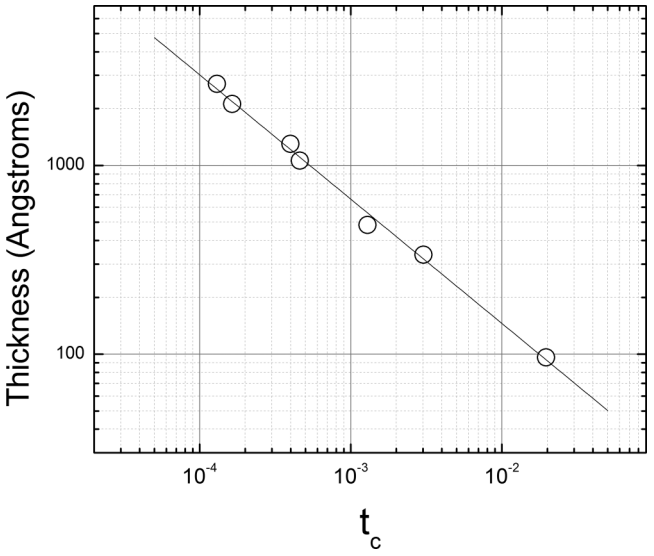

FIG. 10. A plot of planar cell thickness vs critical temperature $t_c = 1 - T_c/T_\lambda$. All data were obtained using AFR. The fit yields a critical exponent $\nu = 0.66 \pm 0.02$ which agrees with the value determined for the bulk superfluid fraction $\nu = 0.6705 \pm 0.0006$ [21].

in addition to this, we see a correlation-length effect which is manifest as a shift of the transition to higher temperatures.

We also note in Fig. 9 the $\times$'s are from the ω_+ mode of the 40-μm cell. As remarked above, except the region where the superfluid density in the ring vanishes, these data follow the relatively smooth drop toward the expected Kosterlitz-Thouless jump. This is the same behavior as the data for the uniform 33.6-nm film. The shift in the transition temperature T_c from ω_+ is plotted in Fig. 10 as a film of 268 nm along with other data available for fully planar confinement in a Si cell (see also Fig. 24 of [31]). All of the data in Fig. 10 have been obtained with AFR. The transition temperature is taken as the last point for which a resonance could be seen. It is clear that the shift in T_c for the ω_+ data agrees well with all the other data from strictly planar cells. Thus, our identification of this signal as coming from the 268-nm region of the Corbino cell is unambiguous. The determination of t_c depends to some extent on the quality of the resonance which is different for different cells, and leads to the scatter one sees in Fig. 10. The film thickness, as determined from the oxide growth, has relatively small uncertainty. The solid line in Fig. 10 is a fit to these data to a power law. It yields the expected shift exponent $\nu = 0.66 \pm 0.02$ which agrees with the value determined for the bulk superfluid fraction $\nu = 0.6705 \pm 0.0006$ [21] and other determinations; see Table I of Ref. [31].

It is interesting to compare the correlation-length effects obtained in the Corbino geometry with the analogous observations in the case of the same thickness film in equilibrium with, and linking an array of $(2\ \mu\mathrm{m})^3$ boxes of helium. These latter data and the arrangement for the measurements are discussed in more detail in [1–3]. In Fig. 11 we plot the superfluid density ratio $\rho_s/\rho_{s,\mathrm{bulk}}$ as a function of temperature. Three sets of data are shown: the Corbino data with $W = 4$ μm; the film-boxes data when the separation of the boxes (these are in a square array) is also 4 μm; and the uniform film data. The influence of the larger confinement on the thin film in equilibrium with it is manifest differently for these two

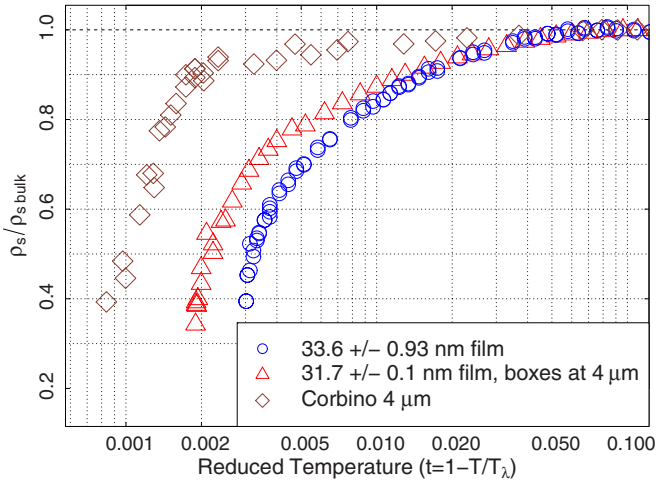

FIG. 11. The ratio ρ_s/ρ_{sb} is plotted for the Corbino cell with $W = 4$ μm as well as for the 33-nm planar cell and the cell with a 31.7-nm film in the presence of $(2\ \mu\text{m})^3$ boxes spaced 4 μm.

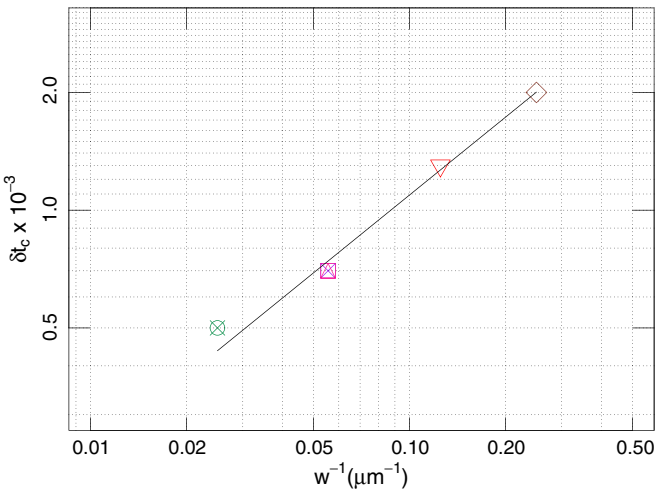

FIG. 12. A plot of δt_c vs W^{-1}. The straight line is given by $\delta t_c \cong (W/\xi_0^-)^{-\nu}$.

arrangements. First of all, in both cases, there is a shift of the transition to higher temperatures. This is larger for the Corbino film. The temperature dependence of $\rho_s/\rho_{s,\text{bulk}}$ is also different for the two cases. For the Corbino case this can be partly understood in terms of Eq. (17). But of course this equation says nothing about a possible shift in T_c. For the boxes-film arrangement the flow within the cell is clearly different. There is no superfluid flow from the boxes into the filling line, as there is for the 0.27-μm region in the Corbino cell. Thus an analysis such as leading to Eq. (17) is not appropriate. It is not clear why the shift in the transition is larger for the Corbino film than in the boxes-film arrangement when the "distance" between the film and the larger reservoirs is the same. This must be related presumably to the perimeter of contact between the large region and the film. There is no theory for helium at present that has addressed these long-range coupling effects.

One can define a shift of the transition temperature $T_c(W)$ for the Corbino data relative to that of a uniform film $T_c(\infty)$, $\delta t_c = [T_c(\infty) - T_c(W)]/T_\lambda$. This shift is shown in Fig. 12 as a function of $1/W$ on a log-log plot. We see that this shift is well described by a power law $\delta t_c = (W/W_0)^{-\nu}$. We find that $W_0 = 0.33$ nm $\cong \xi_0^-$ the coefficient of the bulk correlation length below T_λ. This is a surprising result given the magnitude of W. If W is considered the "small dimension" determining the shift in T_c, then finite-size scaling would predict a dependence of the shift as $W^{-1/\nu}$ not $W^{-\nu}$. Yet the result is clearly in the spirit of finite-size scaling in the sense that no new critical exponent is needed [34] to describe δt_c. Note that the datum for $W = 100$ μm is not plotted on this graph since the shift is too small to be resolved. Extrapolating the line in Fig. 12 to $1/W = 0.01$ μm^{-1} would yield $\delta t_c \cong 10^{-4}$. We also note that this power law must fail as the ring width vanishes. In this limit the maximum shift would be $\sim 2.9 \times 10^{-3}$.

Our Corbino films can be viewed as undergoing a crossover from bulklike behavior far from T_c to finite-size and eventually 2D crossover. One might expect the 2D correlation length to come into play in some way. However the crossover to two dimensions is extremely narrow in temperature. This can be seen as follows. The 2D correlation length below T_c can be defined from the behavior of the dielectric constant associated with vortices and is given by $\xi_{2D}^- = a\exp(1/b\tau^{1/2})$ [20], where one takes $a = \xi_{3D}^-(t)$ and where $\tau \equiv (1 - T/T_c)$, i.e., the distance to the transition temperature T_c not T_λ as for $\xi_{3D}^-(t)$. The nonuniversal constant b depends on the thickness of the film. This was shown by Finotello *et al.* [35,36]. From [36] one obtains that $b(34.5\ \text{nm}) \cong 105$. Thus even for $\tau = 10^{-4}$ one has $\xi_{2D}^- \cong 2.6\xi_{3D}^-$; and, at $\tau = 10^{-3}$ ξ_{2D}^- differs from $\xi_{3D}^-(t)$ by only 30%. Thus, the 2D correlation length not only does not provide a large length scale which might explain our results, but its influence if at all is over a very narrow region of temperature near T_c.

One can now use the shift in the transition temperature to replot the data of Fig. 9 so that the transition takes place at the same temperature as for that of the uniform film, or equivalently that of the 100-μm ring. The data rescaled this way are shown in Fig. 13. There is very good collapse of these data on a universal locus showing the similarity of the behavior for rings of various widths.

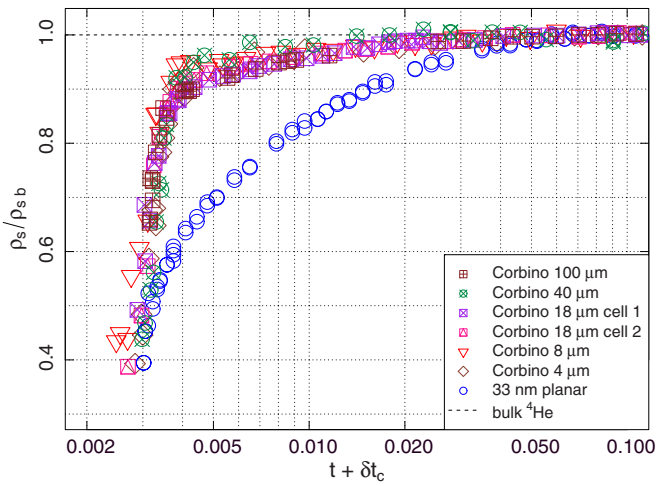

FIG. 13. Scaling of the ratio ρ_s/ρ_{sb} when plotted vs t shifted by $\delta t_c = [T_c(\infty) - T_c(W)]/T_\lambda$.

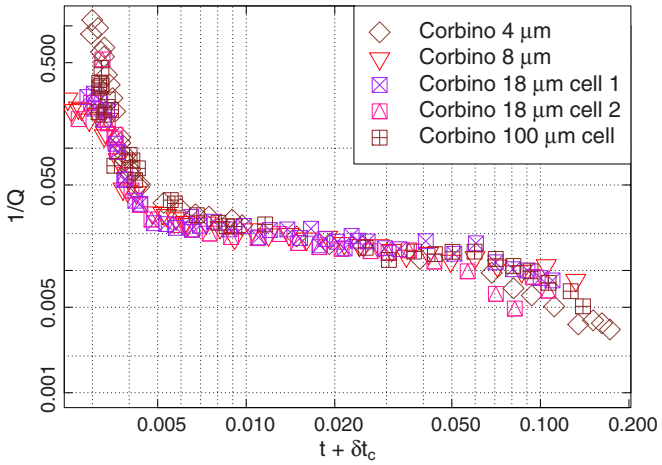

FIG. 14. Scaling of the dissipation $1/Q$ when plotted vs $t + \delta t_c$. This is the same shift as in Fig. 13 for ρ_s/ρ_{sb}.

The analysis of the line shape to obtain the resonant frequency uses Eqs. (30) and (31) derived in [18]. This analysis yields also the dissipation $1/Q$, where Q is the quality factor. A plot of $1/Q$ against the same shifted temperature as for $\rho_s/\rho_{s,\mathrm{bulk}}$ is shown in Fig. 14. We find that the quality factors also collapse onto a single locus near the transition as did $\rho_s/\rho_{s,\mathrm{bulk}}$. Thus, this independent aspect of the transition confirms the scaling with $(W/W_0)^{-\nu}$. To achieve this collapse we have also shifted the dissipation data vertically to agree near $t \cong 0.03$. This is reasonable, since it is our experience with these resonators that each cell has slightly different sources of background dissipation which are not associated with the transition. Some of these come from the flexing of the silicon wafers and depend on the quality of the bonding. One can also see this in Fig. 14 near $t \cong 0.1$, well away from the critical region, that the data do not collapse indicating different sources of background dissipation which depend on the absolute temperature and are not associated with the transition. Note that in Fig. 14 we do not have data for the $W = 40 - \mu$m cell since it did not yield resonances that could be analyzed to extract the quality factor.

V. SUMMARY AND COMMENTS

We have observed that the superfluid fraction of thin films of helium is greatly affected at long range by the proximity of thicker films. For the widest thin film, $W = 100\,\mu$m, for which no significant shift in the transition temperature is observed, the temperature dependence of the measured superfluid fraction can be understood in terms of the hydrodynamics of the two films in equilibrium. The analysis involves a three-chamber Helmholtz oscillator with input from the geometry of the cell and the superfluid fractions of the two films in the thermodynamic limit. When the width of the thinner film is reduced, one finds that the measured superfluid fraction persists to a higher temperature, but its overall temperature dependence is similar to that for the widest film. The shift to higher temperatures is governed by the three-dimensional correlation length. This is surprising in light of the fact that near the transition $W/\xi^-_{3\mathrm{D}} \cong 2400$ to 240 for the widths from 40 to 4 μm. It is found then that both the superfluid fraction and the dissipation associated with the resonance can be collapsed on universal curves. To see how unusual these results are one notes that for a film of thickness H the critical temperature T_c is reached when $H/\xi^-_{3\mathrm{D}}(t_c) \cong 1.7$, and the specific-heat maximum T_m at $H/\xi^-_{3\mathrm{D}}(t_m) \cong 1.5$ [31]. So, these markers of a finite system take place when $\xi^-_{3\mathrm{D}}(t_c) \sim H$. In our case one has $\xi^-_{3\mathrm{D}}(t_c) \ll W$ and the ratio $W/\xi^-_{3\mathrm{D}}$ is not universal because of the $W^{-\nu}$ scaling of δt_c as opposed to $H^{-1/\nu}$ for the planar films. There are clearly different mechanisms at play in finite-size effects for uniform confinement leading to shifts in transition temperatures, or rounding of thermodynamic responses, as opposed to the coupling/proximity effects of the present experiment.

These long-range effects associated with the coupling between two regions of ^{4}He were identified in experiment of the specific heat with $(1\mu\mathrm{m})^3$ boxes of helium separated by a thin film 19 nm thick and 1 μm wide [31,37]. These data presented a puzzle because they did not obey finite-size scaling as the planar films did. Since the connecting film was normal throughout the critical region of the boxes it was felt that the data should represent a collection of isolated boxes, hence should scale. This thinking was clearly wrong. Subsequent data showed that the coupling has nothing to do with the existence of a superfluid, but rather must be a property of the critical system. The observed coupling must be conveyed via critical fluctuations rather than by the existence of a nonzero order parameter. Subsequent measurements with $(2\,\mu\mathrm{m})^3$ boxes where the separation between boxes was varied in two different cells clearly showed this to be the case [31]. Again, as for the now-understood $(1\mu\mathrm{m})^3$ boxes, the coupling of the boxes through the connecting films was observed both below T_λ and above T_λ where the helium was normal. These measurements also showed that there is a reciprocal effect which modifies the connecting film as well as the behavior of helium in the boxes. Of relevance to our present experiment is the observation with these data that the effect of coupling between $(2\,\mu\mathrm{m})^3$ boxes could be seen in the specific heat when the separation between the boxes was as large as 100 times $\xi^+_{3\mathrm{D}}$ for $T > T_\lambda$. Yet the dependence of the excess specific-heat signal generated through this coupling is described by empirical functions which have the same power law as the bulk correlation length $\xi^+_{3\mathrm{D}}$ (see Figs. 19, 21, and 22 in Ref. [3]). We have now seen effects in the Corbino geometry which are manifest at separations of over 1000 times $\xi^-_{3\mathrm{D}}$, yet with a power-law shift in the critical temperature governed by the critical exponent ν of the 3D correlation length.

It is impossible to understand these effects if one thinks in terms of a mean-field transition. This is the approach taken some time ago by Mamaladze and Cheishvili [38,39] in considering the possibility of what would constitute a weak link to couple two regions of helium and display Josephson effects [40]. This mean-field approach does not work for the effects discussed here as has been calculated explicitly [10]. Josephson effects have been seen in both ^{3}He and ^{4}He [41–43]. The former can in fact be considered, as far as its phase transition, a mean-field superfluid. Considerable effort was expended in constructing suitable weak links for these effects. This was aided by the fact that ^{3}He has a relatively large zero-temperature correlation length and of course small

fluctuations effects. In the case of ^{4}He the opposite is true. So that to see Josephson effects for ^{4}He with reasonable weak links one has to work closer to the transition and make use of the divergence of the correlation length. What our data indicate is that coupling between superfluid regions of ^{4}He can be realized over much longer distances than one would expect on the basis of ξ_{3D}. This would make it possible to study Josephson effects with much more readily available weak links separating helium regions as widely as many micrometers. As was pointed out in [3], the experiments with ^{4}He actually take advantage of proximity effects to work with superleaks in a temperature region where, if isolated, they should be normal and hence not support superflow.

In calculations of the winding number for an XY system to obtain ρ_s/ρ one also finds that for films of size $L \times L$ the transition temperature shifts to higher temperatures as L is decreased [44,45]. However, this is an artifact of the periodic boundary conditions, and is seen for films of at most 124×124 atomic sites [46]. Dirichlet boundary conditions on the other hand shift the transition to lower temperatures as the width of the film is decreased [31,47]. This enhancement of the transition temperature and the thermodynamic response, such as specific heat, for periodic boundary conditions in not just a property of 2D XY systems, but was observed for a finite 2D Ising system [48], and in the field-theoretic calculations for ^{4}He with 1D crossover [49]. Our films across the Corbino ring are 5.6×10^5 atoms laterally and 1.1×10^4 to 2.8×10^5 atoms in the flow direction. These are much larger than any numerical calculations. There is no periodicity in the flow direction in our geometry, so the enhancement in ρ_s we measure is not related to this mechanism and must be connected with the 268-nm film on either side of the film in the Corbino ring and critical point coupling.

ACKNOWLEDGMENTS

We are grateful for the support of the National Science Foundation, Grant No. DMR-1101189; the Cornell Nanoscale and Technology Facility, Project No. 526-94; and the Moti Lal Rustgi Professorship Endowment.

[1] J. K. Perron, M. O. Kimball, K. P. Mooney, and F. M. Gasparini, Nat. Phys. **6**, 499 (2010).
[2] J. K. Perron and F. M. Gasparini, Phys. Rev. Lett. **109**, 035302 (2012).
[3] J. K. Perron, M. O. Kimball, K. P. Mooney, and F. M. Gasparini, Phys. Rev. B **87**, 094507 (2013).
[4] M. E. Fisher, Nat. Phys. **6**, 483 (2010).
[5] H. Au-Yang and M. E. Fisher, Phys. Rev. E **88**, 032147 (2013).
[6] H. Au-Yang, Phys. Rev. E **88**, 032148 (2013).
[7] D. B. Abraham, A. Maciołek, and O. Vasilyev, Phys. Rev. Lett. **113**, 077204 (2014).
[8] I. Bozovic, G. Logvenov, M. A. J. Verhoeven, P. Caputo, E. Goldobin, and M. R. Beasley, Phys. Rev. Lett. **93**, 157002 (2004).
[9] A. Del Maestro (private communication).
[10] J. K. Perron and F. M. Gasparini, J. Low Temp. Phys. **162**, 136 (2011).
[11] Y. K. Kwong, K. Lin, M. Park, M. S. Isaacson, and J. M. Parpia, Phys. Rev. B **45**, 9850 (1992).
[12] H. Liu, Z. Ye, Z. Luo, K. Rathnayaka, and W. Wu, Phys. C: Supercond. **468**, 304 (2008).
[13] O. M. Corbino, Nuovo Cim. **1**, 397 (1911).
[14] S. R. D. Thomson, J. K. Perron, M. O. Kimball, S. Mehta, and F. M. Gasparini, J. Vis. Exp. **83**, e51179 (2014).
[15] I. Rhee, F. M. Gasparini, A. Petrou, and D. J. Bishop, Rev. Sci. Instrum. **61**, 1528 (1990).
[16] S. Mehta, M. Kimball, and F. Gasparini, J. Low Temp. Phys. **114**, 467 (1999).
[17] F. M. Gasparini, S. Mehta, and X. Wang, Czech. J. Phys. **46**, 81 (1996).
[18] F. Gasparini, M. Kimball, and S. Mehta, J. Low Temp. Phys. **125**, 215 (2001).
[19] S. Thomson and F. M. Gasparini (unpublished).
[20] V. Ambegaokar, B. I. Halperin, D. R. Nelson, and E. D. Siggia, Phys. Rev. B **21**, 1806 (1980).
[21] L. S. Goldner and G. Ahlers, Phys. Rev. B **45**, 13129 (1992).
[22] D. R. Nelson and J. M. Kosterlitz, Phys. Rev. Lett. **39**, 1201 (1977).
[23] J. W. S. Rayleigh, *The Theory of Sound* (Macmillan, London, 1877).
[24] L. E. Kinsler and A. R. Frey, *Fundamentals of Acoustics* (J. Wiley, New York, 1962).
[25] L. L. Beranek, *Acoustics* (McGraw-Hill, New York, 1954).
[26] J. S. Brooks, B. B. Sabo, P. C. Schubert, and W. Zimmermann, Phys. Rev. B **19**, 4524 (1979).
[27] T.-p. Chen, M. J. DiPirro, B. Bhattacharyya, and F. M. Gasparini, Rev. Sci. Instrum. **51**, 846 (1980).
[28] D. T. Smith, K. M. Godshalk, and R. B. Hallock, Phys. Rev. B **36**, 202 (1987).
[29] F. M. Gasparini and S. Mhlanga, Phys. Rev. B **33**, 5066 (1986).
[30] S. Mehta, Ph.D. thesis, University at Buffalo, State University of New York, 1998.
[31] F. M. Gasparini, M. O. Kimball, K. P. Mooney, and M. Diaz-Avila, Rev. Mod. Phys. **80**, 1009 (2008).
[32] M. O. Kimball and F. M. Gasparini, Phys. Rev. Lett. **86**, 1558 (2001).
[33] I. M. Khalatnikov, *Introduction to the Theory of Superfluidity* (W. A. Benjamin, New York, 1965).
[34] M. E. Fisher, in *Critical Phenomena, Proceedings of the 51st "Enrico Fermi" Summer School, Varenna, Italy*, edited by M. S. Green (Academic Press, New York, 1971).
[35] D. Finotello and F. M. Gasparini, Phys. Rev. Lett. **55**, 2156 (1985).
[36] D. Finotello, Y. Y. Yu, and F. M. Gasparini, Phys. Rev. B **41**, 10994 (1990).
[37] M. O. Kimball, Ph.D. thesis, University at Buffalo, State University of New York, 2005.
[38] Y. G. Mamaladze and O. D. Cheishvili, Zh. Eksp. Teor. Fiz. **50**, 169 (1966) [Sov. Phys. JETP **23**, 112 (1966)].
[39] L. V. Kiknadze, Y. G. Mamaladze, and O. D. Cheishvili, Izmer. Tekh. **7**, 29 (1984) [Meas. Technol. **27**, 607 (1985)].
[40] B. D. Josephson, Phys. Lett. **1**, 251 (1962).

[41] J. C. Davis and R. E. Packard, Rev. Mod. Phys. **74**, 741 (2002).
[42] K. Sukhatme, Y. Mukharsky, T. Chui, and D. Pearson, Nature (London) **411**, 280 (2001).
[43] E. Hoskinson, Y. Sato, and R. Packard, Phys. Rev. B **74**, 100509 (2006).
[44] H. Weber and P. Minnhagen, Phys. Rev. B **37**, 5986 (1988).
[45] E. L. Pollock and D. M. Ceperley, Phys. Rev. B **36**, 8343 (1987).
[46] K. Harada and N. Kawashima, J. Phys. Soc. Jpn. **67**, 2768 (1998).
[47] M. Diaz-Avila, M. Kimball, and F. Gasparini, J. Low Temp. Phys. **134**, 613 (2004).
[48] A. E. Ferdinand and M. E. Fisher, Phys. Rev. **185**, 832 (1969).
[49] W. Huhn and V. Dohm, Phys. Rev. Lett. **61**, 1368 (1988).